IEEE International Symposium on Industrial Electronics (ISIE 2009)
Seoul Olympic Parktel, Seoul, Korea July 5-8, 2009

Biologically inspired Self-adapting Motion Control Employing Neural oscillators

Woosung Yang*, Jaesung Kwon*, Ji-Hun Bae*, Nak Young Chong** and Bum Jae You*
*Center for Cognitive Robotics Research, Korea Institute of Science and Technology, Korea
{wsyang, msrobot, joseph and ybj}@kist.re.kr
**School of Information Science, Japan Advanced Institute of Science and Technology, Japan
nakyoung@jaist.ac.jp

***Abstract*- We address a neural oscillator based control scheme to achieve biologically inspired motion generation. In general, it is known that humans or animals exhibit novel adaptive behaviors regardless of their kinematic configurations against unexpected disturbances or environment changes. This is caused by the entrainment property of the neural oscillator which plays a key role to adapt their nervous system to the natural frequency of the interacted environments. Thus we focus on a self-adapting robot arm control to attain natural adaptive motions as a controller employing the neural oscillator. To demonstrate the excellence of entrainment, we implement the proposed control scheme to a single pendulum coupled with the neural oscillator in simulation and experiment. Then this work shows the performance of the robot arm coupled to neural oscillators in various tasks that the arm traces a trajectory. Exploiting the neural oscillator and its entrainment property, we experimentally verify an impressive capability of biologically inspired self-adaptation behaviors that enables the robot arm to make adaptive changes corresponding to an unexpected environmental variety.**

I. INTRODUCTION

Recently biologically inspired systems and control methods have been studied widely, in particular in robotics field. Thus, a number of virtual human or animal-like robots and control approaches have been yielded for the last decade. Owing that such approaches enable robots to embody autonomous dynamic adaptation motion against unknown environmental changes, its attraction has become generally gained and issued. This is because that the musculo-skeletal system is activated like a mechanical spring by means of the central pattern generators (CPGs) and their entrainment property [1]-[3]. The CPGs consist in the neural oscillator network and produce a stable rhythmic signal. Entrainment of the neural oscillator plays a key role to adapt the nervous system to the natural frequency of the interacted environments incorporating a sensory feedback. Hence, the neural oscillator in the nervous system offers a potential controller, since it is known to be robust and have an entrainment characteristic as a local controller in humans or animals.

Relating these previous works, the mathematical description of a neural oscillator was presented in Matsuoka's works [1]. He proved that neurons generate the rhythmic patterned output and analyzed the conditions necessary for the steady state oscillations. He also investigated the mutual inhibition networks to control the frequency and pattern [2], but did not include the effect of the feedback on the neural oscillator performance. Employing Matsuoka's neural oscillator model, Taga *et al*. investigated the sensory signal from the joint angles of a biped robot as feedback signals [3]-[4], showing that neural oscillators made the robot robust to the perturbation through entrainment. This approach was applied later to various locomotion systems [5]-[7]. In addition to the studies on robotic locomotion [8], more efforts have been made to implement the neural oscillator to a real robot for various applications. Williamson showed the system that had biologically inspired postural primitives [9]. He also proposed the neuro-mechanical system that was coupled with the neural oscillator for controlling its arm [10]. Arsenio [11] suggested the multiple-input describing function technique to evaluate and design nonlinear systems connected to the neural oscillator.

As above, existing works in field of biologically inspired system based on neural oscillators have yielded notable results in many cases. However approaches for a proper behavior generation and complex task were not clearly described due to the difficulty in application considering a real robotic manipulator coupled with the neural oscillator. Yang has presented simulation and experimental results in controlling a robot arm and humanoid robot incorporating neural oscillators [12]-[15]. This work addresses how to control a real system coupled with the neural oscillator for a desired task. For this, real-time feedback is implemented to exploit the entrainment feature of the neural oscillator against unpredictable disturbances.

In the following section, a neural oscillator is briefly explained and its entrainment property is described and verified. Details of the dynamic stability of the developed methodology are discussed in Section III. The experimental results are presented in Section IV. Finally, conclusions are drawn in Section V.

II. RHYTHMIC MOVEMENT USING NEURAL OSCILLATOR

A. Matsuoka's Neural Oscillator

Matsuoka's neural oscillator consists of two simulated neurons arranged in mutual inhibition as shown in Fig. 1 [1]-[2]. If gains are properly tuned, the system exhibits limit cycle behaviours. The trajectory of a stable limit cycle can be derived analytically, describing the firing rate of a neuron with self-inhibition. The neural oscillator is represented by a set of

978-1-4244-4349-9/09/$25.00 ©2009 IEEE

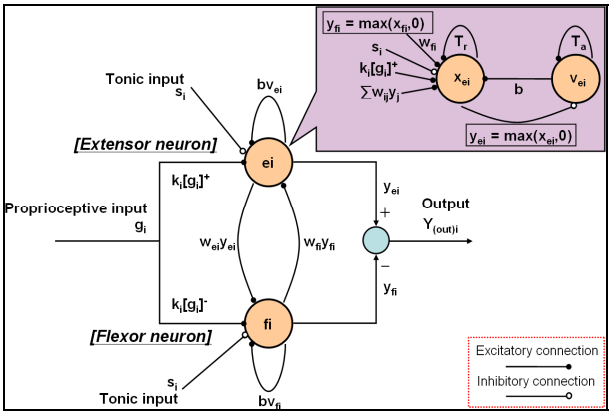

Fig. 1. Schematic diagram of Matsuoka Neural Oscillator

nonlinear coupled differential equations given as

$$\begin{aligned} T_r\dot{x}_{ei} + x_{ei} &= -w_{fi}y_{fi} - \sum_{j=1}^{n} w_{ij}y_j - bv_{ei} - \sum k_i[g_i]^+ + s_i \\ T_a\dot{v}_{ei} + v_{ei} &= y_{ei} \\ y_{ei} &= [x_{ei}]^+ = \max(x_{ei},\ 0) \\ T_r\dot{x}_{fi} + x_{fi} &= -w_{ei}y_{ei} - \sum_{j=1}^{n} w_{ij}y_j - bv_{fi} - \sum k_i[g_i]^- + s_i \\ T_a\dot{v}_{fi} + v_{fi} &= y_{fi} \\ y_{fi} &= [x_{fi}]^+ = \max(x_{fi},\ 0),(i = 1,\ 2,\ \cdots,\ n) \end{aligned} \tag{1}$$

where $x_{e(f)i}$ is the inner state of the i-th neuron which represents the firing rate; $v_{e(f)i}$ represents the degree of the adaptation, modulated by the adaptation constant b, or self-inhibition effect of the i-th neuron; the output of each neuron $y_{e(f)i}$ is taken as the positive part of x_i, and the output of the whole oscillator as $Y_{(out)i}$; w_{ij} (0 for $i \neq j$ and 1 for $i=j$) is the weight of inhibitory synaptic connection from the j-th neuron to the i-th neuron, and w_{ei}, w_{fi} are also weights from the extensor neuron to the flexor neuron, respectively; $w_{ij}y_i$ represents the total input from the neurons inside the network; the input is arranged to excite one neuron and inhibit the other, by applying the positive part to one neuron and the negative part to the other; T_r and T_a are time constants of the inner state and the adaptation effect of the i-th neuron, respectively; s_i is the external input, and g_i indicates the sensory input from the coupled system which is scaled by the gain k_i.

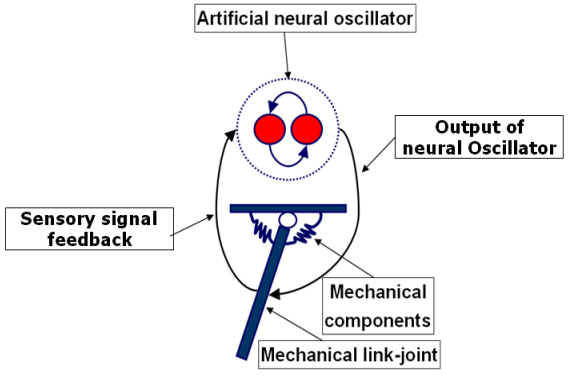

Fig. 2. Mechanical system coupled to the neural oscillator

Figure 2 shows two types of mechanical systems connected to the neural oscillator. The desired torque signal to the i-th joint can be given by

$$\tau_i = k_i(\theta_{vi} - \theta_i) - b_i\dot{\theta}_i, \tag{2}$$

where k_i is the stiffness of the joint, b_i the damping coefficient, θ_i the joint angle, and θ_{vi} is the output of the neural oscillator that produces rhythmic commands of the i-th joint. The neural oscillator follows the sensory signal from the joints, thus the output of the neural oscillator may change corresponding to the sensory input. This is what is called "entrainment" that can be considered as the tracking of sensory feedback signals so that the mechanical system can exhibit adaptive behavior interacting with the environment.

B. Entrainment Property of Neural Oscillator

Generally, it has been known that the Matsuoka's neural oscillator exhibits the following properties: the natural frequency of the output signal increases in proportion to $1/T_r$. The magnitude of the output signal also increases as the tonic input increases. T_r and T_a have an effect on the control of the delay time and the adaptation time of the entrained signal, respectively. Thus, as these parameters decrease, the input signal is well entrained. And the minimum gain k_i of the input signal enlarges the entrainment capability, because the minimum input signal is needed to be entrained appropriately in the range of the natural frequency of an input signal. In this case, regardless of the generated natural frequency of the neural oscillator and the natural frequency of an input signal, the output signal of the neural oscillator locks onto an input signal well in a wide range.

Figure 3 illustrates the entrainment procedure of the neural oscillator. If we properly tune the parameters of the neural oscillator, the oscillator exhibits the stable limit cycle behaviors. In Figure 1, the gain k of the sensory feedback was sequentially set as 0.02, 0.2 and 0.53 such as Figure 3 (a), (b) and (c). When k is 0.02, the output of the neural oscillator can't entrain the sensory signal input as shown in Figure 3 (a). The result of Figure 3 (b) indicates the signal partially entrained. If the gain k is properly set as 0.53, the neural oscillator produces the fully entrained signal as illustrated in Figure 3 (c) in contrast to the result of Figure 3 (b).

C. Verification of Entrainment Property through Experiment

In this subsection, we experimentally verify the entrainment capability of the neural oscillator and its validation addressed in above subsection. As illustrated in Fig. 2, the single pendulum is tightly coupled with the neural oscillator. This means that the neural oscillator observes and entrains the encoder value of the motor in terms of the sensory feedback and, the output of the neural oscillator drives the motor directly. Hence, the pendulum is excited periodically by the output generated in the neural oscillator. And also the coupled oscillator-pendulum exhibits natural adaptive motions even though we swing the pendulum arbitrary 22s to 38s and 56s to 74s sequentially as shown in Fig. 5. It can be confirmed from

the experimental result that entrainment of the neural oscillator enables the coupled system to show naturally self-adapting motions against unpredictable disturbances.

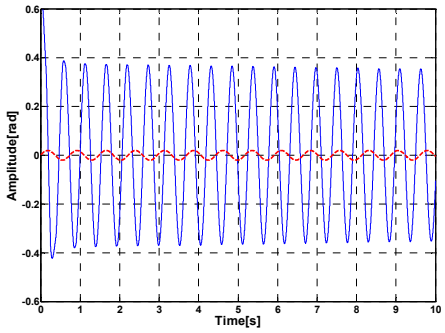

(a)

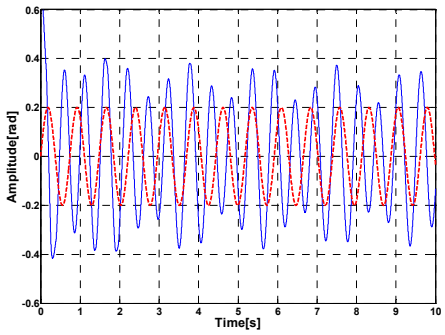

(b)

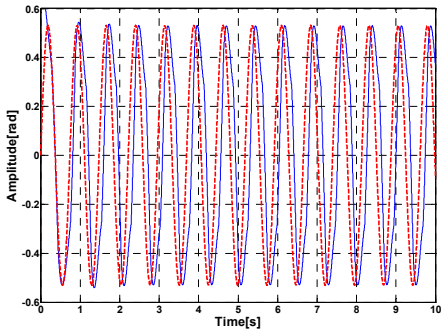

(c)

Fig. 3. Simulation results on the entrainment property of the neural oscillator. The solid line is the output of the neural oscillator and the dashed line indicates the sensory signal input.

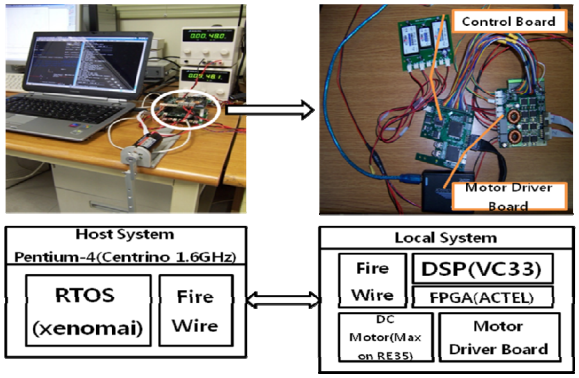

Fig. 4. Experimental setup for driving the single pendulum coupled with the neural oscillator; This operating system runs at 200Hz in real time.

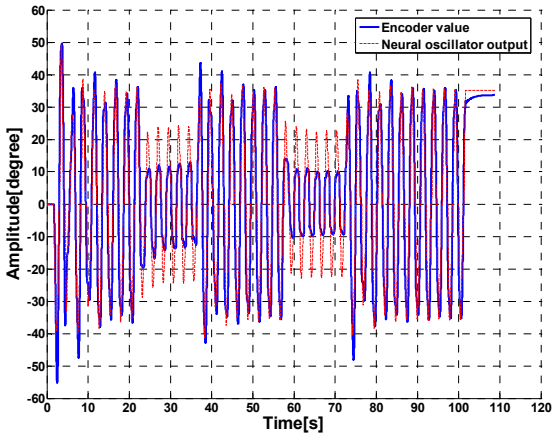

Fig. 5. Experiment result on self-adapting motions of the coupled oscillator -pendulum. The red line is the encoder value and the dashed line indicates the output of the neural oscillator.

III. Control Scheme Based on Neural Oscillator

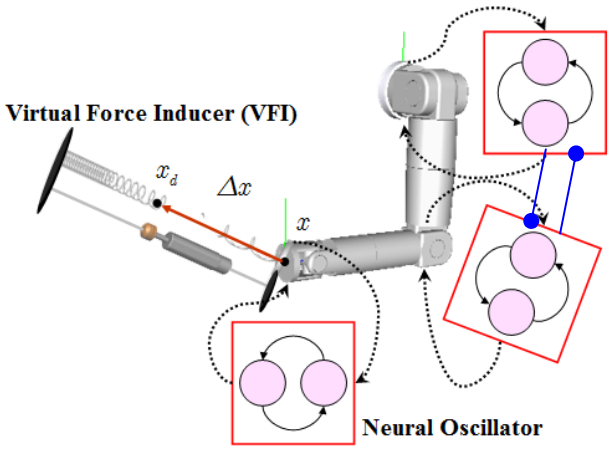

Fig. 6. Schematic robot arm control model coupled with neural oscillators

The neural oscillator is a non-linear system, thus it is generally difficult to analyze the dynamic system when the oscillator is connected to it. Therefore we only analyze the stability of the inner dynamics of the neural oscillator (see Appendix). Also a graphical approach known as the describing function analysis has been proposed earlier [16]. The main idea is to plot the system response in the complex plane and find the intersection points between two Nyquist plots of the dynamic system and the neural oscillator. The intersection points indicate limit cycle solutions. However, even if a rhythmic motion of the dynamic system is generated by the neural oscillator, it is usually difficult to obtain the desired motion required by the task. This is because many oscillator parameters need to be tuned, and different responses occur according to the inter-oscillator network. Hence, we propose the control method that enables a robot system to perform a desired motion without precisely tuning parameters of the neural oscillator within the range of its well-known stable condition.

Figure 6 illustrates a schematic model of a robot arm whose each joint is coupled to the neural oscillators. And a virtual

force leads the coupled robot arm to a given motion. The virtual force inducer (VFI) such as springs and dampers which is supposed to exist virtually at the end-effector of a manipulator can be transformed into equivalent torques. This causes the end-effector of a robot arm to draw according to the desired trajectory calculating position error. Also, it is shown that ill-posedness of inverse kinematics can be resolved in a natural way using without introducing any artificial optimization criterion [17]-[18]. However, even in such a method kinematic configurations including redundant joints may not be guaranteed, even though the posture of a robot arm could be set only within a certain boundary.

From this point of view, it would be advantageous if neural oscillators are hardly coupled to each joint of a robot arm. When the oscillators are implemented to a robotic arm, they provide a proper motor command considering the movements of the joints with sensory signals. Since biologically inspired motions of each joint as described in section II are attained by entrainment of the neural oscillator, the coupled joint can respond intuitively according to environmental change or unknown disturbance inputs performing an objective motion. In addition, each neural oscillator can be tuned in order to give the criterion for limitation of motion within a driving range to the joints considering the amplitude of the sensory feedback signal.

In general, dynamics of a robot system with n-th DOFs could be expressed as

$$H(q)\ddot{q}+\left\{\frac{1}{2}\dot{H}(q)+S(q,\dot{q})\right\}\dot{q}+g(q)=u, \tag{3}$$

where H denotes the $n\times n$ inertia matrix of a robot, the second term in the right hand side of Eq.(3) stands for coriolis and centrifugal force, and the third term is the gravity effect. Then a control input for a rhythmic motion of the dynamic system shown in Eq. (3) is introduced as follows;

$$u=-C_0\dot{q}-J^T(k\Delta x+\varsigma\sqrt{k}\dot{x})-k_o\Delta q+g(q), \tag{4}$$

where

$$C_0=\mathrm{diag}(c_1,\ c_2,\ \cdots,\ c_n)$$

$$c_i=\varsigma_0\sqrt{k}\sqrt{\sum_{j=1}^{n}\left|H_{ij}\right|},\ (i=1,\ 2,\ \cdots,\ n)$$

$$\Delta x=x-x_d$$

$$\Delta q=q-q_{od}$$

where k and ς_0 is the spring stiffness and damping coefficient, respectively for the virtual components. C_0 is the joint damping. k_o and q_{odi} are the stiffness gain and the output of the neural oscillator that produces rhythmic commands, respectively.

The control inputs as seen in Eq. (4) consist of two control schemes. One is based on Virtual spring-damper Hypothesis [17]-[18] and the other is determined in terms of the output of the neural oscillator as illustrated in Eq. (2). In the control input of Eq. (4), the first term describes a joint damping for restraining a certain self-motion which could be occurred in a robot system with redundancy, and the second term means PD control in task space by using of Jacobian transpose, and also a spring and a damper in the sense of physics. Appropriate selection of the parameters such as joint damping factors C_0, stiffness k and damping coefficient ς renders the closed-loop system dynamics convergent, that is, x is converged into x_d and both of $\dot{x}$ and $\dot{q}$ are become 0 as time elapses. In general, the neural oscillators coupled to the joints perform the given motion successively interacting with a virtual constraint owing to the entrainment property, if gains of the neural oscillator are properly tuned [12]-[13]. In the proposed control method, the VFI is considered as a virtual constraint. Also, the coupled model enables a robotic system to naturally exhibit a biologically inspired motion employing sensory signals obtained from each joint under an unpredictable environment change.

Then, closed-loop dynamics with Eq. (3) and Eq. (4) is expressed as

$$H(q)\ddot{q}+\left\{\frac{1}{2}\dot{H}(q)+S(q,\dot{q})+C_0\right\}\dot{q}+J^T(k\Delta x+\varsigma\sqrt{k}\dot{x}) \tag{5}$$
$$+k_o\Delta q=0$$

The inner product between $\dot{q}$ and the closed-loop dynamics of Eq. (5) yields

$$\dot{q}^T\left[H(q)\ddot{q}+\left\{\frac{1}{2}\dot{H}(q)+S(q,\dot{q})+C_0\right\}\dot{q}+J^Tk\Delta x\right. \tag{6}$$
$$\left.+J^T\varsigma\sqrt{k}\dot{x}+k_o\Delta q\right]=0$$

and

$$\frac{d}{dt}E=-\dot{q}^TC_0\dot{q}-\dot{x}^T\varsigma\sqrt{k}\dot{x}\le 0, \tag{7}$$

where E stands for the total energy

$$E(\dot{q},\ \Delta x,\ \Delta q)=\frac{1}{2}\dot{q}^TH(q)\dot{q}+\frac{k}{2}\left\|\Delta x\right\|^2+\frac{k_o}{2}\left\|\Delta q\right\|^2 \tag{8}$$

In Eq. (8), the first term of the quantity E describes the kinetic energy of the robot system, the second term means an artificial potential energy caused by the error Δx in task space and the error Δq gives rise to an artificial potential energy corresponding to the third term in joint space. As it is well known in robot control, the energy balance relation of Eq. (7) shows that the input-output pair $(u,\ \dot{q})$ related to the motion of Eq. (6) satisfies passivity.

IV. Experimental Verification: Opening and Closing a Drawer

For considering the possibility of the proposed control scheme described in Section III, a real robot arm with 6 degrees of freedom (see Fig. 7 (b)) are employed and a real time control system is constructed. This arm controller runs at 200Hz and is connected via IEEE1394 for data transmission at

4kHz. ATI industrial automation's Mini40 sensor was fitted to the wrist joint of the arm to detect external disturbances. The appropriate parameters in Table I were used for the neural oscillator. Also Table I illustrates the parameters on the arm dynamics of the real robot. Since the desired motions are generated in the horizontal plane, q_1 and q_3 are set to 90°. The initial values of q_5 and q_6 are set to 0°, respectively. q_2 and q_4, corresponding to θ_1 and θ_2 in Fig. 7 (a), respectively, are controlled by the neural oscillators. We performed extensive experiments to evaluate the proposed control scheme described in section III.

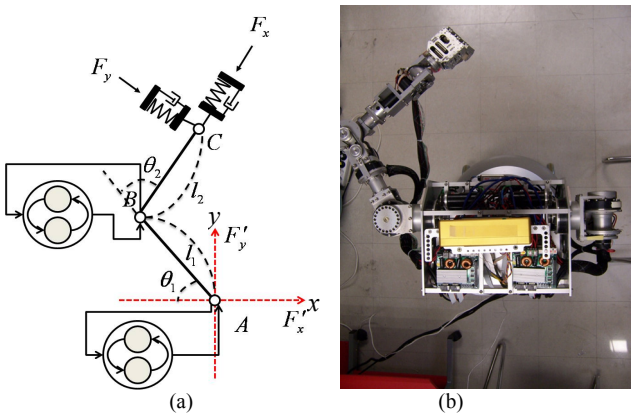

(a) (b)

Fig. 7. (a) Schematic robot arm model and (b) real robot arm coupled with the neural oscillator for experimental test

TABLE I
PARAMETERS OF THE NEURAL OSCILLATOR & ROBOT ARM MODEL

Initial parameters			
Neural oscillator(1)		Neural oscillator(2)	
Inhibitory weight (w_1)	1.7	Inhibitory weight (w_2)	1.7
Time constant (T_{r1})	0.68	Time constant (T_{r2})	0.7
Time constant(T_{a1})	1.36	Time constant(T_{a2})	1.4
Sensory gain (k_1)	3.1	Sensory gain (k_2)	15.6
Tonic input (s_1)	1.0	Tonic input (s_2)	1.0
Robot Arm Model			
Mass 1 (m_1)	2.347kg	Mass 2 (m_2)	0.834kg
Inertia 1 (I_1)	0.0098kgm^2	Inertia 2 (I_2)	0.0035 kgm^2
Length 1 (l_1)	0.224m	Length 2 (l_2)	0.225m

A. Experimental System

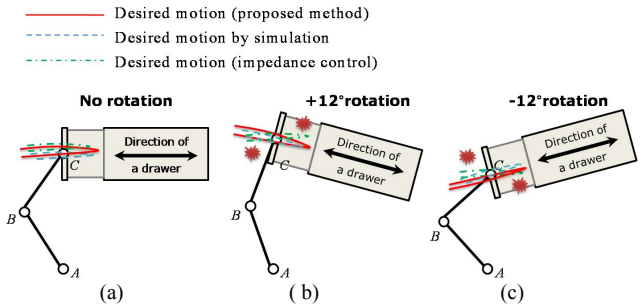

(a) (b) (c)

Fig. 8. Schematic figure on the experiments that robot arm opens and closes a drawer repeatedly. (a) fix the drawer in accordance with the robot arm motion, (b) rotate the drawer clockwise about 12°, (c) rotate the drawer counter-clockwise about 12°

Figure 8 conceptually illustrates the objective tasks with experimental setup for the validation of the proposed control scheme. We evaluate the entrainment capability of the neural oscillator that enables a manipulator to implement and sustain the given task under various environmental changes. Hence, in order to verify the possibility of such adaptation performance, we apply various circumstances to the coupled oscillator-robot arm with the tasks with respect to opening and closing a drawer as seen in Fig. 8. We tightly joined the end-effector of the robot arm to the drawer. The end-effector's direction of the robot arm is designed in accordance with the direction to open or close the drawer under the condition that the drawer is not rotated but fixed. In Figs. 8 (b) and (c), the drawer was rotated clockwise and counter-clockwise about 12° for considering unknown environmental changes. Then, the end-effector of the robot arm brings about various collision problems with the drawer due to a different direction between the end-effector of the robot arm and the drawer. Now, we will examine what happens in the arm motion on performing the objective task if additive external disturbances exist.

B. Experimental Results

Figures 9 and 10 illustrate the experimental results as the sensory feedback of the neural oscillator is turned off and on, respectively. In the first case, if the drawer isn't moved during 0s to 20s, the desired motion of robot arm is not changed. The first joint (q_2) and the second one (q_4) are actuated to move to the distance corresponding to external forces. Hence, if the drawer rotates about +12° and -12° during 20s to 40s and 40s to 60s, the robot arm's motion is autonomously altered. As shown in Figs 9 and 10, the end-effector of the robot arm draws the trajectories corresponding to the desired motion for opening and closing the drawer. The straight dotted lines indicate the desired trajectories of the robot arm generated by simulation. The blue lines show the measured trajectories of the end-effector of the robot arm in experiments. In Fig. 9, movements of the robot arm are identical with the expected performance although there exist inefficient motions due to unknown disturbances. This is because that the desired input of each joint is modified adequately by the impedance model (see Figs. 6 and 7(a)) even though the sensory information of the neural oscillators isn't fed again. In comparison with this, the robot arm coupled with the neural oscillator exhibits the superior potential in a self-adapting motion exploiting the sensory feedback of the neural oscillator for the capability of entrainment. This means that a proper desired motion according to environmental changes is yielded and more efficient motions are led. Such the effect could be accomplished owing that the oscillator based control reproduces the desired joint input entraining the coupled joint motion through the sensory feedback with regard to joint information. The snap shots in Fig. 11 show the robot arm motions implementing the proposed control based on neural oscillator, where we can observe that the end-effector traces the rotated drawer direction.

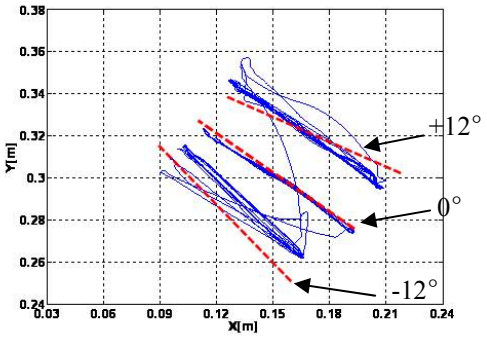

Fig. 9. Trajectories of the end-effector of the robot arm in case that the sensory feedbacks are turned off

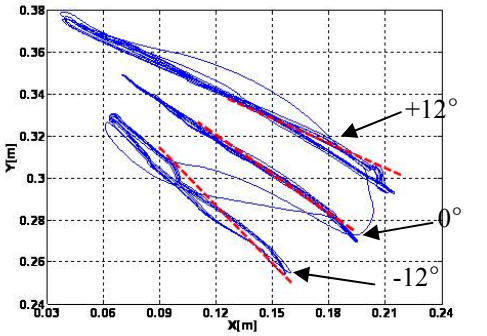

Fig. 10. Trajectories of the end-effector of the robot arm in case that the sensory feedbacks are turned on

For showing the superiority of the biologically inspired control approach, we perform more complex task employing 6-DOF motion of the robot arm. Fig. 12 shows the behavior of the robot arm with respect to opening a door. In the same manner, the task can be attained simply regardless of the desired motion generation for each joint of 6-DOF robot arm coupled with neural oscillators. Because the arm is so compliant, the tracking error is absorbed in the arm compliance. Thus, the robot can open the door easily even under an imprecise desired motion and the unfixed mechanical constraint between the knob of the door and the end-effector of the robot arm as seen in Fig. 14. In addition, though a desired task changes unexpectedly, the entrainment function of the neural oscillator adjusts the control commands in an adaptive way so as to maintain given movements.

V. CONCLUSION

We have presented a control scheme for technically achieving a biologically inspired self-adapting robotic motion. In contrast to existing works that were only capable of rhythmic pattern generation for simple tasks, our approach allowed the robot arm to precisely trace a trajectory correctly through entrainment. With this, the proposed method is verified through more complex behaviors of the real robot arm under unknown environmental changes. Also our approach causes appropriate desired motions irrespective of precisely modelling with respect to external disturbances. For such reason, it was observed from experimental results that the novel adaptive motions corresponding to an external force appear clearly. This approach will be extended to a more complex task toward the realization of biologically inspired robot control architectures.

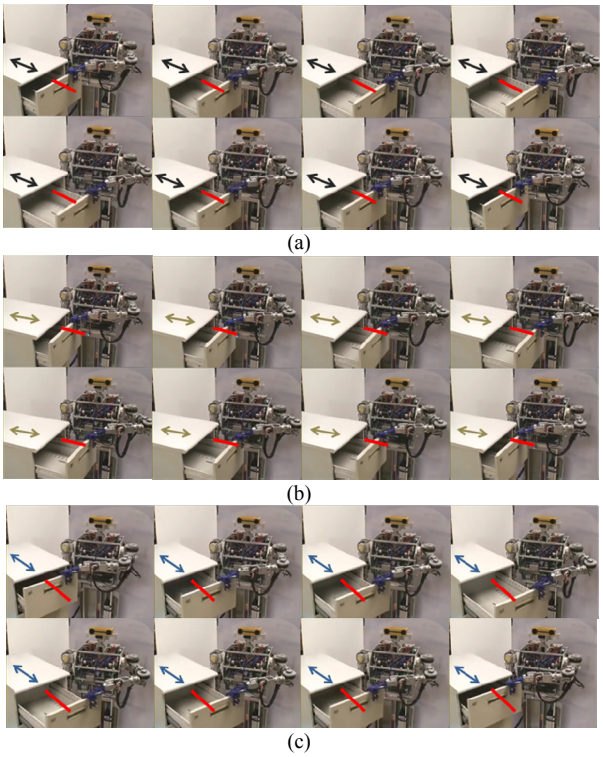

Fig. 11. Snap shots of the robot arm motion in the proposed control method, (a) under 0° rotation of the drawer, (b) under -12° rotation of the drawer, (c) under +12° rotation of the drawer

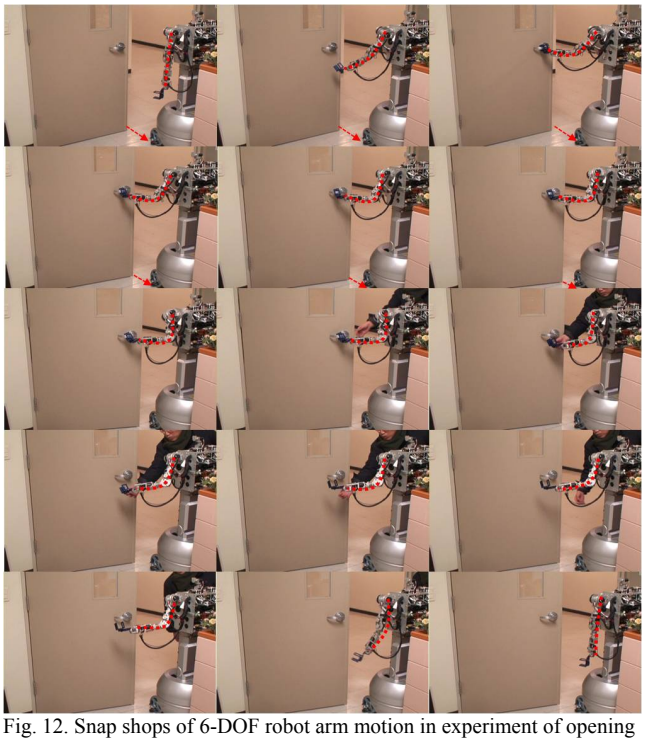

Fig. 12. Snap shops of 6-DOF robot arm motion in experiment of opening a door

APPENDIX

Matsuoka neural oscillators have nonlinearities such as max(x, 0) and min(x, 0). Here, we analyze the dynamics of the neural oscillator on stability in time domain analysis. Equation (1) of the neural oscillator gives as

$$\begin{aligned}\frac{dx_e}{dt} &= g_e(x_e, v_e, x_f, v_f)\\ \frac{dv_e}{dt} &= f_e(x_e, v_e, x_f, v_f)\\ \frac{dx_f}{dt} &= g_f(x_e, v_e, x_f, v_f)\\ \frac{dv_f}{dt} &= f_f(x_e, v_e, x_f, v_f)\end{aligned} \tag{9}$$

where g_e, f_e, g_f and f_f are nonlinear functions of x_e, v_e, x_f and $v_f = \dot{x} = dx_e/dt$. Eq. (9) can be rewritten as

$$\begin{Bmatrix}\dot{x}_e\\ \dot{v}_e\\ \dot{x}_f\\ \dot{v}_f\end{Bmatrix} = \begin{bmatrix}a_{11} & a_{12} & a_{13} & a_{14}\\ a_{21} & a_{22} & a_{23} & a_{42}\\ a_{31} & a_{32} & a_{33} & a_{43}\\ a_{41} & a_{42} & a_{43} & a_{44}\end{bmatrix}\begin{Bmatrix}x_e\\ v_e\\ x_f\\ v_f\end{Bmatrix} \tag{10}$$

where

$$a_{11} = \left.\frac{\partial g_e}{\partial x_e}\right|_{(0,0,0,0)} \quad a_{12} = \left.\frac{\partial g_e}{\partial v_e}\right|_{(0,0,0,0)} \quad a_{13} = \left.\frac{\partial g_e}{\partial x_f}\right|_{(0,0,0,0)} \quad a_{14} = \left.\frac{\partial g_e}{\partial v_f}\right|_{(0,0,0,0)}$$

$$a_{21} = \left.\frac{\partial f_e}{\partial x_e}\right|_{(0,0,0,0)} \quad a_{22} = \left.\frac{\partial f_e}{\partial v_e}\right|_{(0,0,0,0)} \quad a_{23} = \left.\frac{\partial f_e}{\partial x_f}\right|_{(0,0,0,0)} \quad a_{24} = \left.\frac{\partial f_e}{\partial v_f}\right|_{(0,0,0,0)}$$

$$a_{31} = \left.\frac{\partial g_f}{\partial x_e}\right|_{(0,0,0,0)} \quad a_{32} = \left.\frac{\partial g_f}{\partial v_e}\right|_{(0,0,0,0)} \quad a_{33} = \left.\frac{\partial g_f}{\partial x_f}\right|_{(0,0,0,0)} \quad a_{34} = \left.\frac{\partial g_f}{\partial v_f}\right|_{(0,0,0,0)}$$

$$a_{41} = \left.\frac{\partial f_f}{\partial x_e}\right|_{(0,0,0,0)} \quad a_{42} = \left.\frac{\partial f_f}{\partial v_e}\right|_{(0,0,0,0)} \quad a_{43} = \left.\frac{\partial f_f}{\partial x_f}\right|_{(0,0,0,0)} \quad a_{44} = \left.\frac{\partial f_f}{\partial v_f}\right|_{(0,0,0,0)}$$

The solutions of Eq. (10) are expected to be geometrically similar to those of Eq. (9). We assume the solution of Eq. (10) in the form

$$\begin{Bmatrix}x_e\\ v_e\\ x_f\\ v_f\end{Bmatrix} = \begin{Bmatrix}X_e\\ V_e\\ X_f\\ V_f\end{Bmatrix} e^{\lambda t} \tag{11}$$

where X_e, V_e, X_f, V_f and λ are constants. Substitution of Eq. (11) into Eq. (10) leads to the eigenvalue problem

$$\begin{bmatrix} -\frac{1}{T_r}-\lambda & -\frac{b}{T_r} & \left\{-\frac{w}{T_r}\right\}_{x_f>0} & 0\\ \left\{\frac{1}{T_a}\right\}_{x_e>0} & -\frac{1}{T_a}-\lambda & 0 & 0\\ \left\{-\frac{w}{T_r}\right\}_{x_e>0} & 0 & -\frac{1}{T_r}-\lambda & -\frac{b}{T_r}\\ 0 & 0 & \left\{\frac{1}{T_a}\right\}_{x_f>0} & -\frac{1}{T_a}-\lambda \end{bmatrix}\begin{Bmatrix}X_e\\ V_e\\ X_f\\ V_f\end{Bmatrix} = \begin{Bmatrix}0\\0\\0\\0\end{Bmatrix} \tag{12}$$

The eigenvalue λ_1, λ_2, λ_3 and λ_4 can be found by solving the characteristic equation as

$$\lambda_1, \lambda_2, \lambda_3, \lambda_4 = \frac{1}{2}(p \pm \sqrt{p^2 - 4q}) \tag{13}$$

Let's consider the four cases:

Case (1) – $x_e \geq 0$, $x_f \geq 0$, $g_e = g_f = 1$

Using Eq. (12), we can obtain eigenvalues λ_1, λ_2, λ_3 and λ_4

$$\begin{aligned}\therefore \lambda_{1,2} &= \frac{1}{2T_rT_a}(T_r + (1-w)T_a) \pm \frac{1}{2T_rT_a}\sqrt{(T_r + (1-w)T_a)^2 - 4(b+1-w)T_rT_a}\\ &= -\frac{1}{2}\left(\frac{1}{T_a} + \frac{1-w}{T_r}\right) \pm \frac{1}{2}\sqrt{\left(\frac{1}{T_a} + \frac{1-w}{T_r}\right)^2 - \frac{4(b+1-w)}{T_rT_a}}\end{aligned}$$

where $p_{1,2} = T_r + (1-w)T_a$, and $q_{1,2} = (b+1-w)T_rT_a$,

$$\begin{aligned}\therefore \lambda_{3,4} &= -\frac{1}{2T_rT_a}(T_r + (1+w)T_a) \pm \frac{1}{2T_rT_a}\sqrt{(T_r + (1+w)T_a)^2 - 4(b+1+w)T_rT_a}\\ &= -\frac{1}{2}\left(\frac{1}{T_a} + \frac{1+w}{T_r}\right) \pm \frac{1}{2}\sqrt{\left(\frac{1}{T_a} + \frac{1+w}{T_r}\right)^2 - \frac{4(b+1+w)}{T_rT_a}}\end{aligned}$$

where $p_{3,4} = T_r + (1+w)T_a$, and $q_{3,4} = (b+1+w)T_rT_a$,

We can notice that

i) if $(p^2 - 4q) < 0$, the motion is oscillatory;
ii) if $(p^2 - 4q) > 0$, the motion is aperiodic;
iii) if $p > 0$, the system is unstable;
iv) if $p < 0$, the system is stable;

Investigating the stability of the inner dynamics of the neural oscillator exploiting above four conditions,
Case (1-1) – λ_1 and λ_2, λ_3 and λ_4 are Real and Distinct ($p^2 > 4q$).

And also, we assume that the general solutions corresponding to eigenvalues, respectively as follows

$$\begin{aligned}\alpha(t) &= \alpha_0 e^{\lambda_1 t},\ \beta(t) = \beta_0 e^{\lambda_2 t}\\ \gamma(t) &= \gamma_0 e^{\lambda_3 t},\ \delta(t) = \delta_0 e^{\lambda_4 t}\end{aligned} \tag{14}$$

where α_0, β_0, γ_0 and δ_0 are the initial values of α, β, γ and δ respectively.

The type of motion depends on whether λ_1 and λ_2, λ_3 and λ_4 are of the same sign or of opposite sign. If λ_1 and λ_2, λ_3 and λ_4 have the same sign.

In ($q_{1,2} > 0$)

$$(b+1-w)T_rT_a > 0 \quad (\because T_r, T_a > 0) \quad \therefore b > w-1$$

and ($q_{3,4} > 0$)

$$(b+1+w)T_rT_a > 0 \quad (\because T_r, T_a > 0) \quad \therefore b > -w-1$$

Namely, $b > \max(-w-1, w-1)$, the equilibrium point is called a node. The phase plane diagram for the case $\lambda_1 < \lambda_2 < 0$ and $\lambda_3 < \lambda_4 < 0$ (when λ_1 and λ_2, λ_3 and λ_4 are real and negative or $p_{1,2}$ and $p_{3,4} < 0$)

In ($p_{1,2} < 0$)

$$T_r + (1-w)T_a < 0 \Rightarrow 1 - w < -\frac{T_r}{T_a} \qquad \therefore w > \frac{T_r}{T_a} + 1$$

and ($p_{3,4} < 0$)

$$T_r + (1+w)T_a < 0 \Rightarrow 1 + w < -\frac{T_r}{T_a} \qquad \therefore w < -\frac{T_r}{T_a} - 1$$

Namely,

$$w < -1 - \frac{T_r}{T_a} \ or\ w > +1 + \frac{T_r}{T_a}$$

In this case, Eq.(14) shows that all the trajectories tend to the origin as $t \to \infty$ and hence the origin is called a stable node. On the other hand, if $\lambda_1 > \lambda_2 > 0$ ($p_{1,2} > 0$) and $\lambda_3 > \lambda_4 > 0$ ($p_{3,4} > 0$),
In ($p_{1,2} > 0$)

$$T_r + (1-w)T_a > 0 \Rightarrow 1 - w > -\frac{T_r}{T_a} \qquad \therefore w > \frac{T_r}{T_a} + 1$$

and ($p_{3,4} > 0$)

$$T_r + (1+w)T_a > 0 \Rightarrow 1 + w > -\frac{T_r}{T_a} \qquad \therefore w > -\frac{T_r}{T_a} - 1$$

Namely,

$$+1 + \frac{T_r}{T_a} < w < -1 - \frac{T_r}{T_a}$$

Therefore, the origin is called an unstable node. And if time constants, T_r and T_a, are both positive, this condition is impossible.

Case (2) – $x_e \geq 0$, $x_f < 0$, $g_e = 1$, $g_f = 0$

The eigenvalues $\lambda_1, \lambda_2, \lambda_3$, and λ_4 can be found by solving the characteristic equation. And we can obtain below eigenvalues λ_1, λ_2, λ_3 and λ_4

$$\lambda_1 = -\frac{1}{T_a}, \quad \lambda_2 = -\frac{1}{T_r}$$

$$\lambda_3 = -\frac{(T_r + T_a - \sqrt{T_r^2 - 2T_rT_a + T_a^2 - 4T_rT_ab})}{2T_rT_a}$$

$$\lambda_4 = -\frac{(T_r + T_a + \sqrt{T_r^2 - 2T_rT_a + T_a^2 - 4T_rT_ab})}{2T_rT_a}$$

$$\therefore \lambda_{3,4} = -\frac{1}{2T_rT_a}(T_r + T_a) \pm \frac{1}{2T_rT_a}\sqrt{(T_r + T_a)^2 - 4T_rT_a(b+1)}$$

$$= -\frac{1}{2}\left(\frac{1}{T_a} + \frac{1}{T_r}\right) \pm \frac{1}{2}\sqrt{\left(\frac{1}{T_a} + \frac{1}{T_r}\right)^2 - 4\frac{b+1}{T_rT_a}}$$

where $p_{3,4} = T_r + T_a$, and $q_{3,4} = T_rT_a(b+1)$,

Case (2-1) – λ_1 and λ_2, λ_3 and λ_4 are Real and Distinct ($p^2 > 4q$).
If λ_1 and λ_2, λ_3 and λ_4 have the same sign ($q_{3,4} > 0$)

$$T_rT_a(b+1) > 0 \qquad \therefore b > -1$$

Namely, $b > \max(-w-1, w-1, -1)$. This equilibrium point is stable.

Case (3) – $x_e < 0$, $x_f \geq 0$, $g_e = 0$, $g_f = 1$.

This case is similar to the Case (2), and the eigenvalues are the same.

Case (4) – $x_e < 0$, $x_f < 0$, $g_e = g_f = 0$.

The eigenvalues $\lambda_1, \lambda_2, \lambda_3$, and λ_4 can be found by solving the characteristic equation. The stability of this equilibrium point is determined by the eigenvalues,

$$\lambda_{1,2} = -\frac{1}{T_r}, \ \lambda_{3,4} = -\frac{1}{T_a}$$

The equilibrium point is zero, therefore all the trajectories will converge to this equilibrium point and the system does not oscillate.

ACKNOWLEDGMENT

This work was supported by Korea MIC and IITA through IT Leading R&D Support Project. [2009-S028-01, Development of Cooperative Network-based Humanoids Technology]

REFERENCES

[1] K. Matsuoka, "Sustained Oscillations Generated by Mutually Inhibiting Neurons with Adaptation," *Biological Cybernetics*, Vol. 52, pp. 367-376 (1985).

[2] K. Matsuoka, "Mechanisms of Frequency and Pattern Control in the Neural Rhythm Generators," *Biological Cybernetics*, Vol. 56, pp. 345-353 (1987).

[3] G. Taga, Y. Yamagushi and H. Shimizu, "Self-organized Control of Bipedal Locomotion by Neural Oscillators in Unpredictable Environment," *Biological Cybernetics*, Vol. 65, pp. 147-159, (1991).

[4] G. Taga, Y. Yamagushi and H. Shimizu, "Self-organized Control of Bipedal Locomotion by Neural Oscillators in Unpredictable Environment," *Biological Cybernetics*, Vol. 65, pp. 147-159, (1991).

[5] G. Taga, "A Model of the Neuro-musculo-skeletal System for Human Locomotion," *Biological Cybernetics*, Vol. 73, pp. 97-111 (1995).

[6] S. Miyakoshi, G. Taga, Y. Kuniyoshi, and A. Nagakubo, "Three-dimensional Bipedal Stepping Motion Using Neural Oscillators-Towards Humanoid Motion in the Real World," *Proc. IEEE/RSJ Int. Conf. on Intelligent Robots and Systems*, pp. 84-89 (1998).

[7] Y. Fukuoka, H. Kimura and A. H. Cohen, "Adaptive Dynamic Walking of a Quadruped Robot on Irregular Terrain Based on Biological Concepts," *The Int. Journal of Robotics Research*, Vol. 22, pp. 187-202 (2003).

[8] G. Endo, J. Nakanishi, J. Morimoto and G. Cheng, "Experimental Studies of a Neural Oscillator for Biped Locomotion with QRIO," *Proc. IEEE/RSJ Int. Conf. on Intelligent Robots and Systems*, pp. 598-604 (2005).

[9] M. M. Williamson, "Postural Primitives: Interactive Behavior for a Humanoid Robot Arm," *4th Int. Conf. on Simulation of Adaptive Behavior*. MIT Press, pp. 124-131 (1996).

[10] M. M. Williamson, "Rhythmic Robot Arm Control Using Oscillators," *Proc. IEEE/RSJ Int. Conf. on Intelligent Robots and Systems*, pp. 77-83 (1998).

[11] A. M. Arsenio, "Tuning of neural oscillators for the design of rhythmic motions," *Proc. IEEE Int. Conf. on Robotics and Automation*, pp. 1888-1893 (2000).

[12] W. Yang, N. Y. Chong, C. Kim and B. J. You, "Optimizing Neural Oscillator for Rhythmic Movement Control," *Proc. IEEE Int. Symp. on Robot and Human Interactive Communication*, pp. 807-814 (2007).

[13] W. Yang, N. Y. Chong, Jaesung Kwon and B. J. You, "Self-sustaining Rhythmic Arm Motions Using Neural Oscillators," *Proc. IEEE/RSJ Int. Conf. on Intelligent Robots and Systems*, pp. 3585-3590 (2008).

[14] W. Yang, N. Chong, C. Kim and B. J. You, "Entrainment-enhanced Neural Oscillator for Rhythmic Motion Control," *Journal of Intelligent Service Robotics*, pp. 303-311 (2008).

[15] W. Yang, N. Y. Chong, SyungKwon Ra, ChangHwan Kim and B. J. You, "Self-stabilizing Bipedal Locomotion Employing Neural Oscillators," *Proc. IEEE-RAS Int. Conf. on Humanoid Robots*, pp. 8-15 (2008)

[16] Jen-Jacques E. Slotine, Weiping Li, "Applied Nonlinear Control," Englewood Cliffs, N. J., Prentice Hall. (1991).

[17] S. Arimoto, M. Sekimoto, H. Hashiguchi and R. Ozawa, "Natural Resolution of ill-Posedness of Inverse Kinematics for Redundant Robots: A Challenge to Bernstein's Degrees-of Freedom Problem," *Advanced Robotics*, 19: 401-434 (2005).

[18] S. Arimoto, M. Sekimoto, J.-H. Bae and H. Hashiguchi, "Three-dimensional Multi-Joint Reaching under Redundancy of DOFs," *Proc. IEEE/RSJ Int. Conf. on Intelligent Robots and Systems*, 1898-1904 (2005).